Journal of Alloys and Compounds 688 (2016) 288–294

Contents lists available at ScienceDirect

Journal of Alloys and Compounds

journal homepage: http://www.elsevier.com/locate/jalcom

The calorimetric analysis as a tool for studying the aging hardening mechanism of a Cu-10wt%Ni-5.5wt%Sn alloy

M.J. Diánez [b], E. Donoso [a], M.J. Sayagués [b], A. Perejón [b], P.E. Sánchez-Jiménez [b], L.A. Pérez-Maqueda [b], J.M. Criado [b, *]

[a] Departamento de Ciencia de los Materiales, Facultad de Ciencias Físicas y Matemáticas, Universidad de Chile, Casilla 2777, Santiago, Chile
[b] Instituto de Ciencias de Materiales de Sevilla, C.S.I.C., Centro Mixto Universidad de Sevilla-C.S.I.C., Américo Vespucio 49, Isla de la Cartuja, 41092 Sevilla, Spain

ARTICLE INFO

Article history:
Received 10 June 2016
Accepted 3 July 2016
Available online 5 July 2016

Keywords:
Cu-Ni-Sn alloys
DSC and phase transitions
Aging hardening
TEM and ED structural analysis
XRD lattice parameters

ABSTRACT

The transformations of a Cu-10wt%Ni-5.5wt%Sn alloy as a function of the aging time in the range from room temperature up to 600 °C have been followed by Differential Scanning Calorimetry (DSC). The results obtained have shown that this alloy undergone two overlapping exothermic phase transitions with DSC peaks at 208 °C and 305 °C, respectively, followed by an endothermic phase transformation with a DSC peak at 526 °C. The structural analysis by TEM, ED, EDX and XRD of the intermediates phases previously discriminated by DSC suggests that the first exothermic peak is associated to the spinodal decomposition of the sample, while the second one is associated to the segregation of a DO_{22} $(Cu_xNi_{1-x})_3Sn$ tetragonal phase coherent with the α-Cu structure of the starting alloy. The endothermic peak has been associated to the precipitation of cubic DO_3 nanocrystals from the DO_{22} phase previously formed. The microhardness measurements carried out in combination with the structural characterization demonstrate that the aging hardening of the alloy under study is exclusively due to the formation of the coherent DO_{22} phase. The $DO_{22} \rightarrow DO_3$ transition leads to a dramatic drop of the hardness of the alloy.

1. Introduction

The industry is demanding materials exhibiting high strength at high temperatures combined with high electrical and high thermal conductivity. Due to its high electrical and thermal conductivity, copper is a most promising metal for all of these applications. It has the advantage of a low elastic modulus, which minimizes thermal stresses in actively cooled structures [1,2] although its strength has to be increased in order to meet the design requirements for high temperature applications. The method generally used for increasing the copper strength implies to prepare supersaturated solid solution from melting a mixture of copper with small percentage of other metals followed by quenching at room temperature. The hardening is achieved by annealing at the proper temperature for precipitating intermetallic phase. This behavior explains the huge number of papers [3–8] available in literature dealing with the hardening of copper alloys in the Cu rich region. Cu-Ni-Sn alloys have widely used in automotive and aerospace industries and a large number of Cu-Ni-Sn alloys in the copper reach region are available in the market with assigned code numbers included in the Unified Numbering System (UNS) managed jointly by ASTM and the International Society of Automotive Engineers (SAE) [9]. The samples with composition Cu-7.5 wt % Ni- 5 wt % Sn (UNS code C72650) and Cu-15 wt % Ni-8 wt % Sn (UNS code C72900) are the most widely used because they combine high electrical conductivity, corrosion resistance and toughness required in the electronic industry for bearing, electronic connectors, etc. [10]. It must be pointed out that the evolution of the microstructure of the above Cu-Ni-Sn alloys as far as the aging is in progress have been studied in literature [11–20] and it seems to be generally accepted that these alloys undergo the following successive transformations: 1) Spinodal decomposition, 2) Formation of a metastable γ′-DO_{22} $(Cu_xNi_{1-x})_3Sn$ tetragonal phase coherent with the starting α-phase and 3) The precipitation of a γ-DO_3 fcc cubic structure from the DO_{22} phase. A number of papers have been focused on the study of the phase diagrams for

* Corresponding author. Instituto de Ciencia de Materiales de Sevilla (C.S.I.C.-Univ. Sevilla), C. Américo Vespucio 49, Sevilla 41092, Spain.
E-mail address: jmcriado@icmse.csic.es (J.M. Criado).

http://dx.doi.org/10.1016/j.jallcom.2016.07.021
0925-8388/

stablishing the stability of the above phases as a function of the composition and temperature [21–28]. It is noteworthy to remarks that Cu-Ni-Sn alloys in the copper rich region are marketed as spinodal decomposition hardened alloys [10] because it has been concluded in a number of papers [19,29–31] that the hardening is produced in the early stage of aging due to the decomposition of the original α-supersaturated alloy in two phases Sn-rich and Sn-lean, respectively, but with identical structure. However, there is not agreement in literature concerning to the structural modifications undergone during the aging of these alloys that are really responsible for the hardening. However, some authors [17,19] have concluded that the hardening is associated to the formation of the DO_{22} phase rather than to the spinodal decomposition. However, it is very difficult to show the presence of spinodal decomposition by TEM because the reflections of the DO_{22} phase are very bright and they mask the satellite side band and it has been suggested that both the modulated and the DO_{22} phases would overlap in aged samples [14,32]. López-Hirata et al. [32] have studied by X-ray Diffraction (XRD) the aging at 673 K of Cu-15wt%Ni-8wt% Sn alloys and they have observed very week diffraction peaks closed to the main (200) diffraction peak of the α-phase that they attributed to spinodal decomposition sidebands. However, Sahu et al. [18] have carried out a careful Rietveld structural analysis of an alloy with identical composition and aged at the same temperature of 673 K and they have not found any XRD peak that would be attributed to sidebands, but an XRD peak corresponding to the diffraction of the (311) planes of the γ-DO_3 phase appears at the 2θ reflections attributed to spinodal sideband by López-Hirata et al. [32].

It is worth noting that most of the studies related with the influence of aging on the strengthening of Cu-Ni-Sn alloys have the disadvantage that a parallel study of mechanical properties and structural analysis was not carried out on the same samples. On the contrary, the results obtained by studying the influence of aging on the mechanical properties was explained by taking into account the structural changes reported by other authors under similar aging conditions. It has been shown in previous papers [33–38] that Differential Scanning Calorimetry (DSC) could be a proper tool for discriminating the successive steps taking place during the annealing of alloys as a function of the temperature. The scope of this work is to discriminate by DSC the different thermal effects undergone by a Cu-Ni-Sn alloy at rising temperature combined with microhardness measurements and structural analysis by XRD and TEM in order to elucidate the phase transformations responsible of the improvement of the mechanical properties by aging.

2. Experimental

The alloys were prepared by melting in an induction furnace under inert atmosphere (Ar), from stoichiometric mixtures of high purity copper, nickel and tin. The ingots were homogenized by annealing at 800 °C during 24 h under argon atmosphere before cooling to room temperature. Subsequently, the material was submitted to successive cold-rolling treatments with intermediate annealing of 1 h at 800 °C until reaching a thickness of 3 mm. After the last annealing treatment the material was water quenched for preserving the α-Cu structure of the homogeneous supersaturated solid solution.

The X-ray diffractions diagrams (XRD) were recorded with a PHILPS X'pert Pro equipped with an X'celerator detector and a graphite diffracted beam monochromator. CuKα radiation and a nickel filter were used. A voltage of 40 kV and an intensity of 40 mA were employed. The lattice parameters were determined by fitting the XRD pattern by means of the Rietveld method using the FullProf software.

A DSC TA Instruments, model Q 200, that allow a maximum temperature of 700 °C was used. The DSC diagrams were recorded at a heating rate of 10 °C/min under a nitrogen flow of 100 cc/min.

A simultaneous TG-ATD TA Instruments, model 600, that allows to reach temperatures up to 1509 °C, was used for recording the DTA curves at temperatures higher than 700 °C. The DTA traces were obtained under nitrogen atmosphere at a heating rate of 10 °C/min.

TEM, ED and EDS analysis were performed in a 200 kV microscope (Philips CM200) with a supertwin objective lens and a LaB6 filament (point resolution ~ 0.3 nm) and an EDAX analysis system to measure the chemical composition. The specimens for TEM observation were prepared by cutting discs of 3 mm in diameter from the sample sheets and they were later thinned by dimple (0.5 μm) and ion milling until 100 nm.

Microhardness measurements were performed at room temperature in a high Futur-Tech FM-700 microdurometer employing a load of 2 N during 15 s. Each microhardness value was calculated as an average of 10 microhardness indentations.

3. Results and discussion

Fig. 1a shows the XRD diagram of the as quenched disc of Cu-10Ni-5.5Sn alloy. It can be observed that the sample is constituted by a homogeneous supersaturated alloy with α-Cu structure covered by a surface layer of $CuNiO_4Sn$ that is easily removed after a gently polishing as shown in Fig. 1b. The Rietveld analysis of the XRD diagram of the polished sample has shown that the best fitting is obtained by considering preferred orientations through the (100) lattice planes as shown in Fig. 2. The lattice parameter determined from Rietveld refinement (Table 1) is $a = 3.6406$ Å in good agreement with the value expected for an alloy of this composition [13,18].

Fig. 3 shows the TEM and ED observation for the starting quenched sample. The sample wash thinned by ion milling bombardment of only one side of the disc in order to get information of the bulk and the surface composition. TEM micrograph of Fig. 3 shows the formation of large number of dislocations that could be generated from the quenching of the sample from 800 °C. The Electron Diffraction Pattern (EDP) of the supersaturated alloy shows two phases, one with the microstructure of α-Cu single crystals of the phase oriented along the $[011]_{Cu}$ zone axis (dot EDP), which agree with the crystal orientation forecasted from XRD

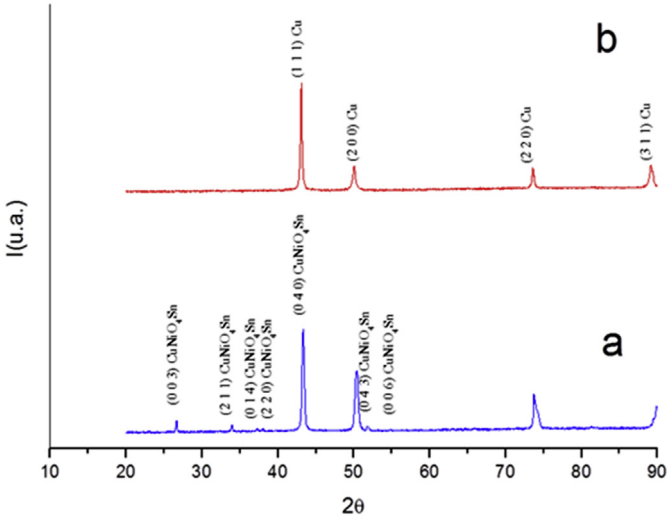

Fig. 1. XRD diagrams of the as prepared homogeneous Cu-10Ni-5.5Sn alloy: a) as prepared; b) after gently surface polishing.

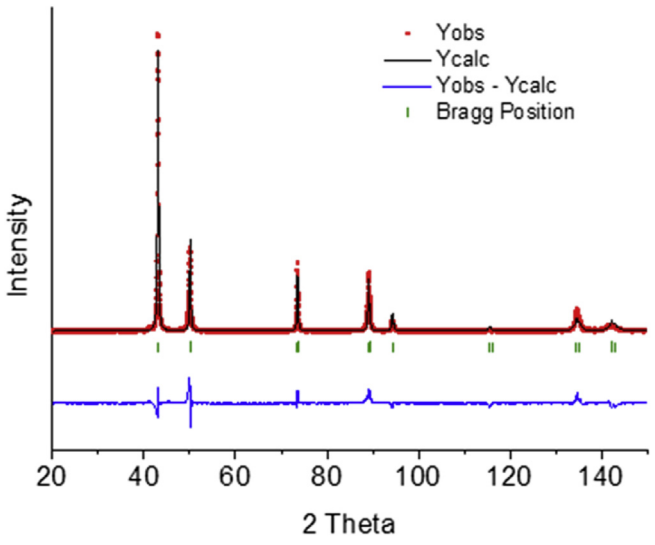

Fig. 2. Fitting of the XRD diagram of the starting simple by assuming (100) preferring orientations.

Table 1
Vickers microhardness (Hv) and lattice parameters (a) of the Cu-10Ni-5.5Sn alloy as a function of the annealing temperature.

Annealing temperature (°C)	Hv	a (Å)
As prepared	117 (±8)	3.6406 (0.010)
200	128 (±5)	3.6430 (0.002)
250	146 (±5)	3.6316 (0.002)
300	256 (±8)	3.6334 (0.007)
350	312 (±6)	3.6246 (0.005)
450	303 (±7)	3.6164 (0.001)
550	176 (±12)	3.6176 (0.009)
750	118 (±10)	3.6366 (0.001)
800	121 (±11)	3.6409 (0.003)

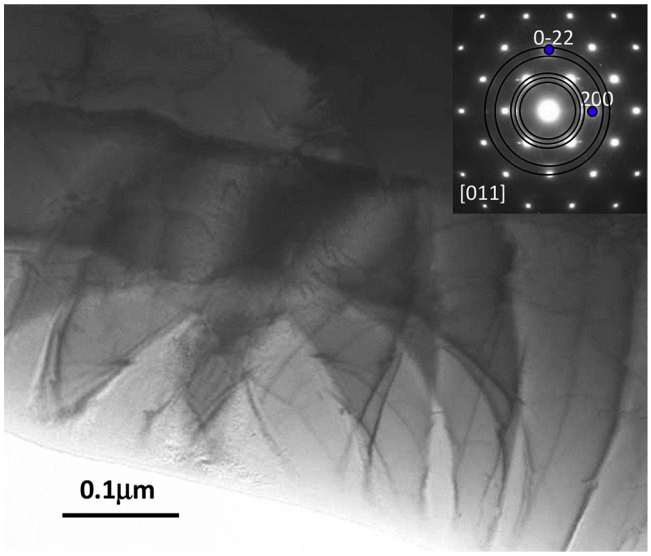

Fig. 3. TEM micrograph and the corresponding EDP of the Cu-10Ni-5Sn alloy before aging.

Rietveld analysis. The second phase corresponds to $CuNiO_4Sn$ with nanocrystalline structure (ring EDP, JPDF file 004-836) that would be associated to the surface oxidation layer originated during the tempering of the sample layer according with the XRD results previously reported and disappears after polishing. It is noteworthy to point out that the results that will be shown from now were obtained from polished samples in which the surface layer of $CuNiO_4Sn$ was removed.

Fig. 4 shows the DSC obtained under flow of nitrogen at a heating rate of 10 °C/min. No weight change of the sample was observed along the DSC experiments, which indicate that no oxidation took place and the sample preserved its metallic brightness. Fig. 4 clearly shows two exothermic peaks at 208 °C and 305 °C as well as an endothermic peak at 560 °C that must be associated to phase transformations undergone by the sample during the heating cycle. Similar results were previously reported by Lourenço and Santos [39] by studying the aging hardening of a Cu-9wt%Ni-6wt%Sn alloy. They observed two overlapping exothermic peak at temperatures lower than 400 °C associated to an increase of the hardness and an endothermic peak at temperatures ranging from about 440 °C to 530 °C, depending of the previous aging treatment of the sample, that was associated to a drastic hardness diminution. These authors concluded that the hardening was due to the precipitation of a γ-DO_3, while the endothermic peak was attributed to the redissolution of the equilibrium γ-DO_3 precipitates previously formed for regenerating the starting α-supersaturated solution, although neither XRD nor TEM structural analyses were reported for confirming these conclusions. However, it must be pointed out that the thermodynamic stabilization of the supersaturated solution would require temperatures in the range 700–800 °C, according to the Cu-Ni-Sn isopleths calculated by Zhao and Notis from the ternary phase diagrams for compositions around 10% of nickel [14,15]. The solvus temperatures proposed by Lourenço and Santos [39] are in strong disagreement with the values expected from the phase diagrams and, therefore, a structural analysis in combination with DSC and microhardness measurements would be required for understanding the aging hardening mechanism of Cu-Ni-Sn alloys.

Fig. 5 shows the TEM micrograph and the EDP of a sample annealed at 200 °C for two hours that is in the range of the peak temperature of the first endothermic peak shown in Fig. 4. The XRD diagram recorded for this sample was quite similar to the one included in Fig. 1b and no sideband were observed. The EDP shows the microstructure of a single crystal of the α copper phase oriented along $[011]_{Cu}$. Moreover, the lattice parameter determined from Rietveld fitting, included in Table 1, does not show the diminution with regards to the starting sample that would be expected if a

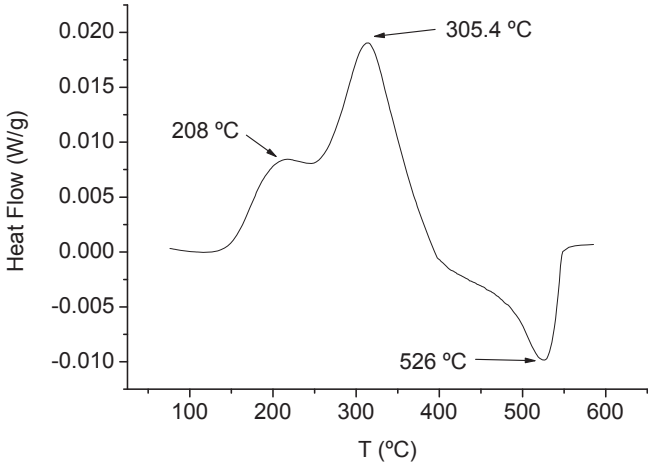

Fig. 4. DSC of the Cu-10Ni-5.5 Sn obtained under flow of nitrogen at a heating rate of 10 °C/min.

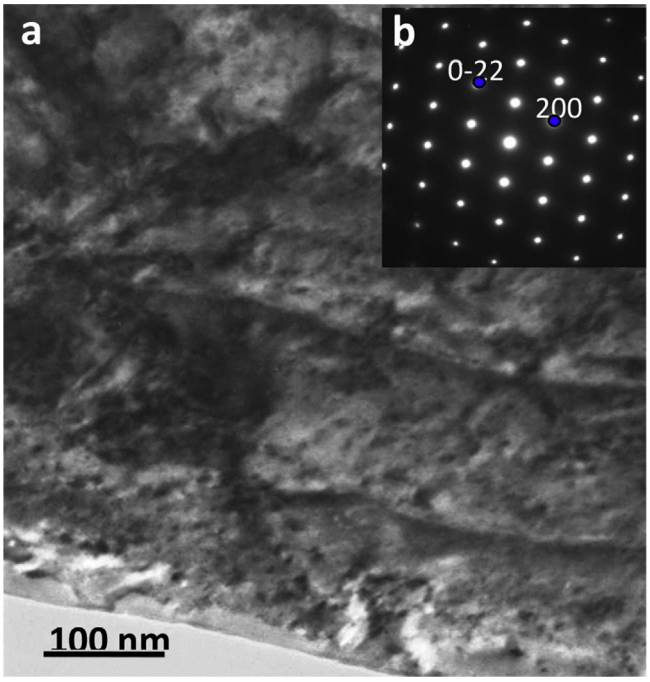

Fig. 5. TEM micrograph and the corresponding EDP along [011]Cu of the Cu-10Ni-5Sn aged at 200 °C.

phase segregation would take place. However, the invariance of the lattice parameter associated to the first exothermic peak would be compatible with a spinodal phase transition, provided that it implies the decomposition of the supersaturated solid solution into Sn-rich and Sn-lean phases with identical α-copper structure. It has been shown [14] that it is very difficult to observe in these alloys the sidebands typical of modulated structure, but the TEM picture reported in Fig. 5 point out the formation of parallel strips that would be attributed to the generation of a modulated structure. Thus, the first DSC exothermic peak in Fig. 4 could be interpreted by assuming that a spinodal decomposition of the Cu-10Ni-5.5Sn alloy has taken place leading to a modulated structure that maintains the same [011] zone axis orientation reported for the starting supersaturated solid solution.

Superstructure diffraction spots were observed in the Electron Diffraction patterns obtained for the sample annealed by two hours at 350 °C that is inside the temperature range of the second DSC exothermic peak. Thus, several lattice sections were obtained varying the g vector in order to identify the source and crystal structure if the superlattice present in the sample. Four of these EDPs regions and their corresponding schemes are shown in Fig. 6, where the black dots belong to the cubic α-Cu subcell (**Fm3m**) and the color dots to superstructure diffractions. The analysis of the superstructure maxima in the $\mathbf{[001]_{Cu}}$ zone axis show the following different features: $\{½\ 1\ 0\}_{Cu}$ and $\{1\ 0\ 0\}_{Cu}$ positions elongated along $(0\ k\ 0)$ reciprocal direction (red spots); $\{1\ ½\ 0\}_{Cu}$ and $\{0\ 1\ 0\}_{Cu}$ positions elongated along $(h00)_{Cu}$

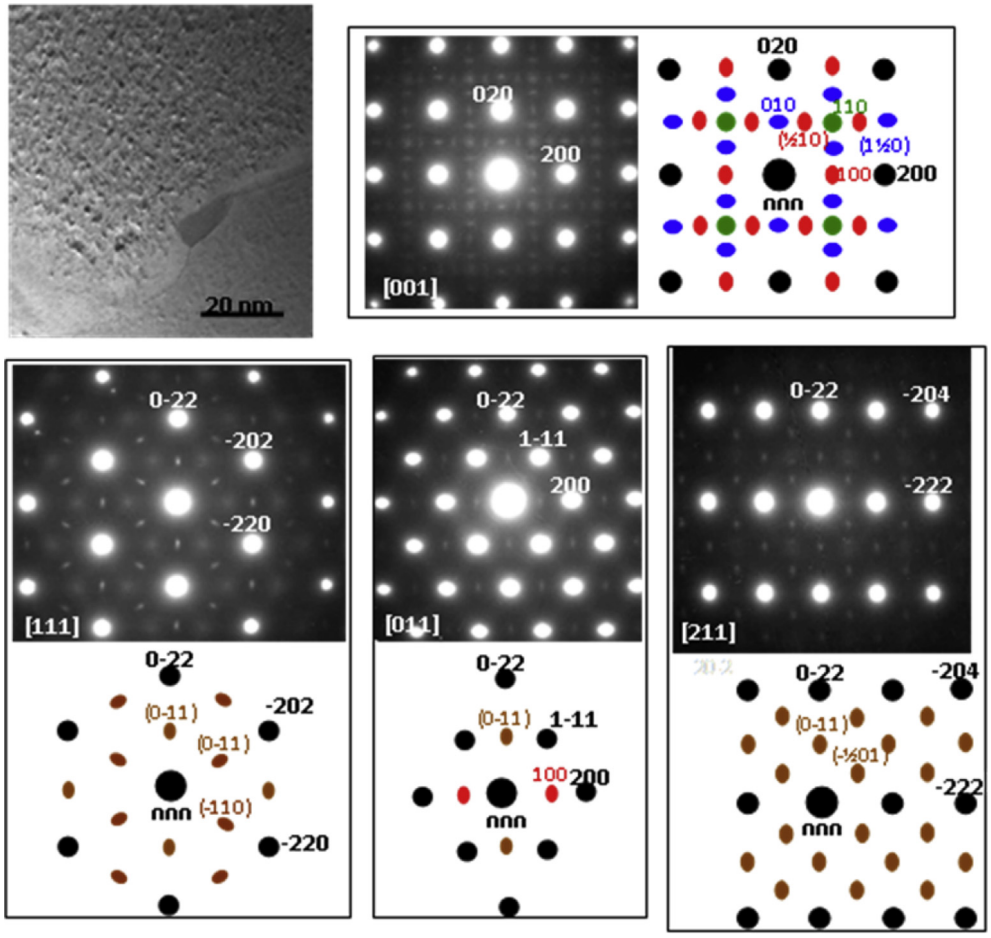

Fig. 6. TEM and EDPs results corresponding to the Cu-10Ni-5.5Sn alloy aged at 350 °C. The ED patterns along four different zones axis show superstructure maxima related with DO_{22}- $(Cu,Ni)_3Sn$ phase.

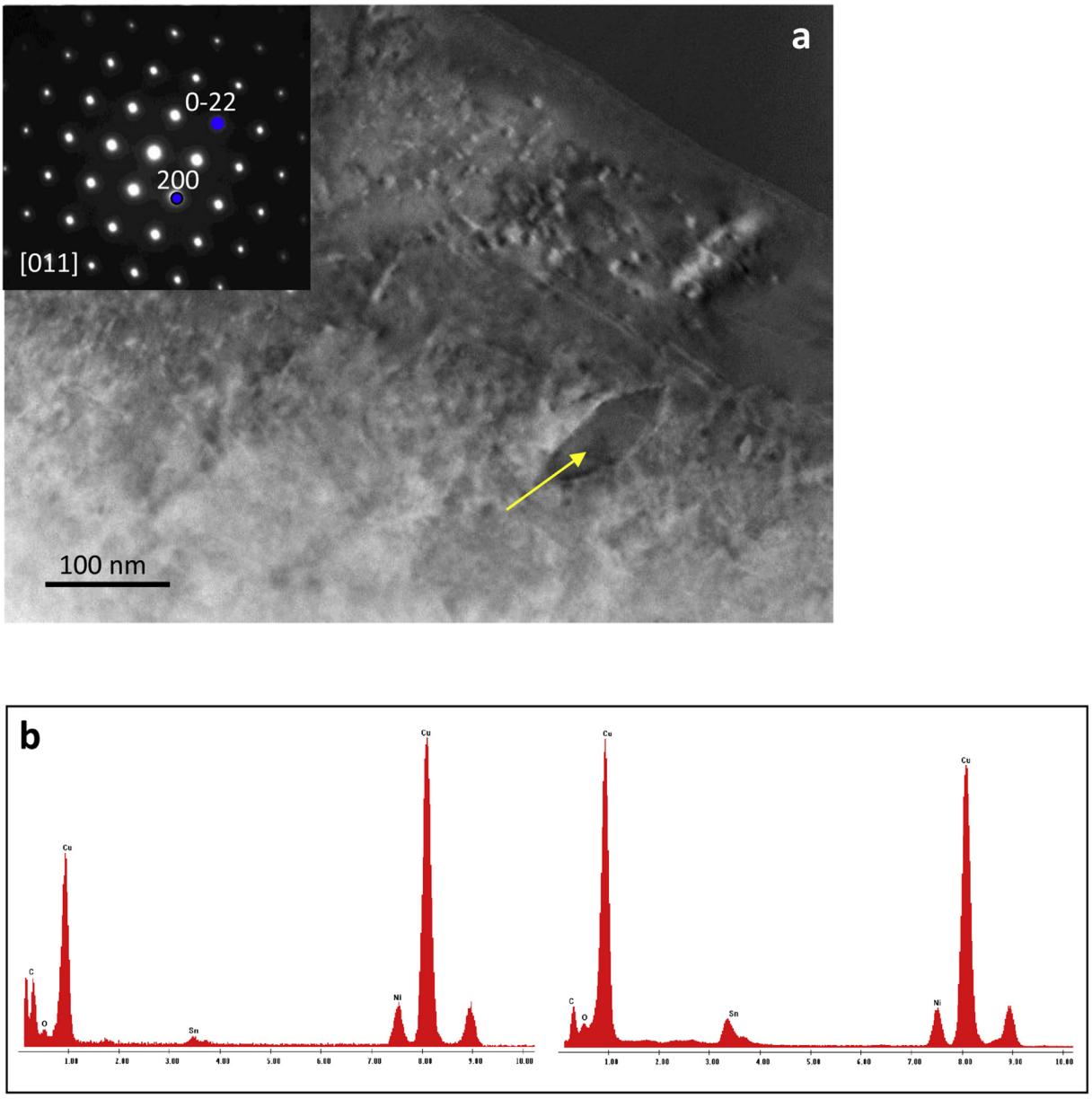

Fig. 7. (a) TEM micrograph and the corresponding EDP along [011]Cu of the Cu-10Ni-5Sn alloy after aging at 550 °C. (b) EDX analysis taken from two areas with different Sn composition. The arrow show the area of the acicular precipitate at which an enrichment of nickel and tin has been observed.

reciprocal direction (blue spots) and $\{1\ 1\ 0\}_{Cu}$ positions that appear without elongation (green spots). The elongation of the diffraction maxima indicates that the superstructure is disordered in the respective reciprocal directions. Moreover, the four order superlattice along $\{2\ 4\ 0\}_{Cu}$ reflexions expected for the DO_{22} structure [11] has been observed as well. On the other hand, the **$[0\,1\,1]_{Cu}$**, **$[1\,1\,1]_{Cu}$** and **$[2\,1\,1]_{Cu}$** zone axis show superstructure diffraction maxima in {0−1 1} positions that are elongated along the $(0\ h\ h)_{Cu}$ reciprocal direction (brown marked) in addition to the positions marked in red previously described. In the **$[2\,1\,1]_{Cu}$** zone axis appears the scattered dot at $\{-½\ 0\ 1\}_{Cu}$ indicating again the four order superstructure along $(204)_{Cu}$ characteristic of the DO_{22} structure. Taking into account that this phase have a composition $(Cu_xNi_{1-x})_3$ Sn with a structure A_3B, all the superstructure maxima can be indexed according to a tetragonal supercell described by the stacking of atoms on the $\{240\}_{Cu}$ planes of the Cu *fcc* lattice where every four planes contain only B atoms in good agreement with the results previously reported by Barburaj et al. [11].

The ED structural analysis previously reported suggests that the second peak of the DSC diagram of Cu-10%Ni-5.5Sn alloy shown in Fig. 4 is associated to the formation of a $(Cu_xNi_{1-x})_3$ Sn DO_{22} phase. It is clear that the formation of this phase would necessary imply the segregation of Cu and Sn from the supersaturated solid solution leading to a decrease of the lattice parameter that would approach to the lattice parameter of α-copper. Thus, the lattice parameter for the bulk sample has been determined from Rietveld fitting of the XRD of the sample annealed at 350 °C. The result included in Table 1 point out a clear diminution of the lattice parameter, supporting that a segregation of nickel and/or Sn for generating the DO_{22} phase has taken place.

Finally, a TEM study of a sample withdrawn from the DSC after reaching a temperature of 550 °C was carried out for characterizing the phase transition associated to the third endothermic peak in

Fig. 4. The TEM picture and ED pattern shown in Fig. 7 point out that the superstructures of the DO_{22} phase coherent with the alloy matrix have disappeared at the time that precipitation of elongated particles are observed (marked with an arrow on Fig. 7). The ED pattern taken along the [110] axis of the α-Cu cell in the area of the precipitated particle included in Fig. 7 shows a *fcc* cubic structure that would be on agreement with the structure expected for the γ-DO_3 precipitates proposed in literature [11,14,18,40]. The EDX elemental analyses carried out in the matrix and in the area closed to the precipitate are also shown in Fig. 7.

The results included in Fig. 7 point out that Ni and Sn were present in the matrix, but their concentrations were higher near the marked particle, which again supports that the formation of γ-DO_3 precipitates could be the phase transition associated to the endothermic peak reported in Fig. 4. It is noteworthy to take into account that Lourenço and Santos [39] have attributed the endothermic peak to the redissolution of DO_3 precipitates although these authors did not carried out a structural characterization for confirming this hypothesis. The determination of the lattice parameter of the sample annealed at 550 °C would contribute to the correct assignation of the endothermic peak in Fig. 4. This is because the redissolution of previously segregated phases would lead to an increase of the lattice parameter until recovering the value of the homogeneous solid solution. The value of the lattice parameter *a* determined from Rietveld fitting of the XRD diagram of the sample annealed at 550 °C is included in Table 1. It can be observed that a noticeably increase of the lattice parameter for recovering the starting value $a = 3.6406$ Å have not been not taken place. This behavior suggests that the endothermic peak is not really associated to a redissolution process, but to the precipitation of γ-DO_3 crystal from the previously formed DO_{22} coherent phase.

The above conclusion would be also supported by taking into account that, according with the phase diagrams of the system Cu-Ni-Sn [14,15], the solvus temperature for the formation of supersaturated solid solution with composition around Cu-10Ni-5.5Sn is in the range 700–800 °C. The maximum temperature allowed by the DSC equipment here used is 700 °C. Thus, a high temperature DTA apparatus has been used for obtaining additional information regarding to the solvus temperature of this alloy. Fig. 8 shows that the DTA obtained under inert atmosphere for the sample previously annealed until 550 °C clearly display a strong exothermic peak at 767 °C that is in the temperature range expected for the

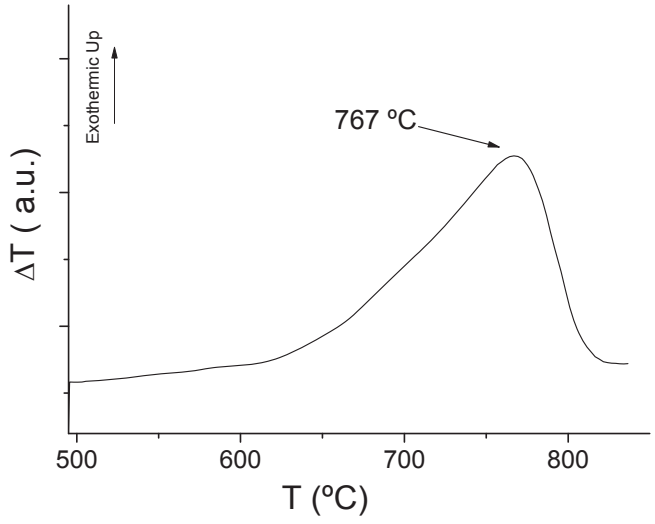

Fig. 8. DTA obtained under flow of nitrogen at a heating rate of 10 °C/min for a Cu-10Ni-5.5 Sn sample previously annealed at 550 °C.

solvus temperature of a Cu-10Ni-5.5Sn alloy at which the homogeneous solid solution is thermodynamically stable. Moreover the lattice parameter determined from the Rietveld fitting of the XRD diagram of the sample withdrawn from the DTA equipment after being heated up to 800 °C, shown in Table 1, reproduces again the value expected for the homogeneous solid solution. This result demonstrates that the redissolution of the precipitates really occur at temperatures higher than 700 °C.

It is noteworthy to point out that an overall enthalpy equal to −20.8 J/g has been determined for the two overlapping exothermic peaks, while an enthalpy equal to 6.8 j/g has been calculated for the endothermic peak. In summary, the total enthalpy evolved from the starting supersaturated solid solution until overpassing the temperature of the last endothermic peak in Fig. 4 is equal to −14 J/g. Thus, the overall precipitation process, taking place in three successive steps, is exothermic as would be expected, provided that the homogeneous solid solution is not thermodynamically stable in the range of temperatures shown in Fig. 4. The fact that the $DO_{22} \rightarrow$ γ-DO_3 phase transition, associated to the last DSC peak in Fig. 4, is endothermic clearly shows that the DO_{22} phase is more stable than the γ-DO_3 phase. These results confirm the proposal of author authors [12,14] that consider that the stabilization of the metastable DO_{22} phase takes place because of the similar lattice sizes of this phase and the *fcc* phase of the supersaturated solid solution that minimizes the strains during the *fcc*→DO_{22} transition. However, it has been reported here by the first time that an increase of the enthalpy of the system is required for overcoming the large lattice mismatch associated to the $DO_{22} \rightarrow$ γ-DO_3 conversion.

Finally, the HV hardness have been measured for a set of samples annealed at different temperatures in the range of the successive thermal effects observed in the DSC shown in Fig. 4 in order to discern which of the phases generated along the heat treatment leads to the aging hardening of the sample. For this purpose a set of different samples were placed in the DSC equipment and submitted to a heating rate of 10 °C/min and withdrawn from the device after reaching temperatures previously selected along the peaks corresponding to the successive phase transformations observed by DSC. The values of HV obtained at different temperatures are included in Table 1 together with the corresponding values of the lattice parameters as determined from Rietveld fitting. These results demonstrate that the initial hardness of the starting Cu-10Ni-5.5Sn alloy is maintained in the temperature range of the first DSC peak, but a dramatic increase of the hardness, accompanied by a diminution of the lattice parameters, takes place as far as the second DSC peak is in progress. This hardness increase is followed by a drastic drop of this parameter as soon as the annealing temperature reaches the zone at which the endothermic DSC peak in Fig. 4 is taking place. These results clearly show that the aging hardening of Cu-10Ni-5.5Sn is not a direct consequence of the spinodal decomposition but it is due to the subsequent formation of a $(Cu_x$-$Ni_{1-x})_3Sn$ DO_{22} phase coherent with the α- Cu structure of the supersaturated solid solution.

4. Conclusions

The calorimetric study of alloy by DSC together with the study of the structural changes and the mechanical properties changes associated to the phase transitions undergone by a Cu-10wt%Ni-5.5wt%Sn, as reported by DSC, supports the following conclusions:

1. The DSC analysis of the homogeneous Cu-10wt%Ni-5.5wt%Sn alloy allows to discriminate the following successive phase transitions: α-Cu → γ′-DO_{22} → DO_3 taking place as a function of the annealing temperature.

2. The endothermic character of the γ'-DO_{22} → DO_3 phase clearly demonstrates the higher thermal stability of the metastable γ'-DO_{22} coherent phase, embedded into the α-Cu framework, with regards to the DO_3 precipitates.
3. The study of the mechanical properties of the Cu-10wt%Ni-5.5wt%Sn after undergoing every one of the above described phase transformations suggest that the noticeably aging improvement of the mechanical properties rest solely on the formation of the γ'-DO_{22} phase.
4. The results here reported clearly show that DSC could be a powerful tool for discerning the transformations undergone by the alloys as a function of the temperature that would help to determine the connections between the transitions observed and the changes of properties associated to them.

Acknowledgement

The authors would like to acknowledge the facilities provided by the Instituto de Ciencia de Materiales de Sevilla (Spain) and the Departamento de Ciencia de Materiales of the University of Chile (Chile).

References

[1] I. Anzel, A.C. Kneissl, L. Kosec, Internal oxidation of rapidly solidified ternary copper alloys part I: a new model of dispersoids formation, Z. Met. 90 (1999) 621–629.
[2] G. Yang, Z. Li, Y. Yuan, Q. Lei, Microstructure, mechanical properties and electrical conductivity of Cu-0.3Mg-0.05Ce alloy processed by equal channel angular pressing and subsequent annealing, J. Alloys Compd. 640 (2015) 347–354.
[3] Q. Feng, L.N. Song, Y.W. Zheng, Y.T. Fang, L. Meng, J.B. Liu, H.T. Wang, Evolution of fcc/bcc interface and its effects on the strengthening of severe drawn Cu-3wt% Cr, J. Alloys Compd. 640 (2015) 45–50.
[4] W. Chrominski, M. Lewandowska, Precipitation phenomena in ultrafine grained Al-Mg-Si alloy with heterogeneous microstructure, Acta Mater. 103 (2016) 547–557.
[5] I. Markovic, S. Nestorovic, B. Markoli, M. Premovic, S. Mladenovic, Study of anneal hardening in cold worked Cu-Au alloys, J. Alloys Compd. 658 (2015) 414–421.
[6] T. Hu, J.H. Chen, J.Z. Liu, Z.R. Liu, C.L. Wu, The crystallographic and morphological evolution of the strengthening precipitates in Cu-Ni-Si alloys, Acta Mater. 61 (2013) 1210–1219.
[7] X.P. Ding, H. Cui, J.X. Zhang, H.X. Li, M.X. Guo, Z. Lin, L.Z. Zhuang, J.S. Zhang, The effect of Zn on the age hardening response in an Al–Mg–Si alloy, Mater. Des. 65 (2015) 1229–1235.
[8] X.N. Li, M. Wang, L.R. Zhai, C.M. Bao, J.P. Chu, C. Dong, Thermal stability of barrierless Cu-Ni-Sn films, Appl. Surf. Sci. 297 (2014) 89–94.
[9] B. Robert, Ross in Metallic Materials Specification Handbook, fourth ed., vol. 1, Springer Science+ Bussiness Media, US, 1992, p. 132.
[10] W. Raymond, M.J. Gedeon, Performances advances in copper-nickel-tin spinodal alloys, Adv. Mater. Proc. 171 (2013) 20–25.
[11] E.G. Barburaj, U.D. Kulkarni, E.S.K. Menon, R. Krishnan, Initial stages of decomposition in Cu-9Ni-6Sn, J. Appl. Cryst. 12 (1979) 476–480.
[12] L. Liu, H. Huang, R. Fu, D. Liu, T.Y. Zhang, DO22-(Cu,Ni)3Sn intermetallic compound nanolayer formed in Cu/Sn-nanolayer/Ni structures, J. Alloys Compd. 486 (2009) 207–211.
[13] S. Spooner, B.G. Lefevre, The effect of prior deformation on spinodal age hardening in Cu-15Ni-8Sn, Metall. Trans. A 11 (1980) 1085–1093.
[14] J.C. Zhao, M.R. Notis, Spinodal decomposition, ordering transformation and discontinuous precipitation in a Cu-15Ni-8Sn alloy, Acta Mater 46 (1998) 4203–4218.
[15] J.C. Zhao, M.R. Notis, Microstructure and precipitation kinetics in a Cu-7.5Ni-5Sn alloy, Scr. Mater. 11 (1998) 1509–1516.
[16] B. Alili, D. Bradai, P. Zieba, On the discontinuous precipitation reaction and solute redistribution in a Cu-15%Ni-8%Sn alloy, Mater. Charact. 59 (2008) 1526–1530.
[17] J.C. Rhu, S.S. Kim, Y.C. Jung, S.Z. Han, C.J. Kim, Tensile strength of thermo-mechanically processed Cu-9Ni-6Sn alloys, Metal. Mater. Trans. A 30 (1999) 2649–2657.
[18] P. Sahu, S.K. Pradham, M. De, X-ray diffraction studies of the decomposition and microstructural characterization of cold-worked powders of Cu-15Ni-Sn alloys, J. Alloys Compd 377 (2004) 103–116.
[19] J.B. Singh, J.G. Wen, P. Bellon, Nanoscale characterization of the transfer layer formed during dry sliding of Cu-15 wt%Ni-8 wt%Sn bronze alloy, Acta Mater 56 (2008) 3053–3064.
[20] P. Kratochvil, J. Mencl, J. Pesicka, S.N. Komnik, The structure and low temperature strength of the age hardened Cu-Ni-Sn alloys, Acta Metall. 32 (1984) 1493–1497.
[21] P. Virtanen, T. Tiainen, T. Lepistö, Precipitation at faceting grain boundaries of Cu-Ni-Sn alloys, Precipitation at faceting grain boundaries of Cu-Ni-Sn alloys, Mater. Sci. Eng. A 251 (1998) 269–275.
[22] K.P. Gupta, An expanded Cu-Ni-Sn system (copper-nickel-zinc), J. Phase Equilib. 21 (2000) 479–484.
[23] J. Miettinen, Thermodynamic description of the Cu-Ni-Sn system at the Cu-Ni side, Comp. Coupling Phase Diag. Thermochim. 27 (2003) 309–318.
[24] G. Gosh, Landolt Bernstein, New Series IV/11C3, MSIT, Springer, Berlin-Heidelberg, 2007.
[25] C. Schmetterer, H. Flandorfer, C.H. Luef, A. Kodentsov, H. Ipser, Cu-Ni-Sn system: a key system for lead free soldering, J. Electron. Mater 38 (2009) 10–24.
[26] C.H. Lin, S.W. Chen, C.H. Wang, Phase equilibria and solidification properties of Sn-Cu-Ni alloys, J. Electron. Mater 31 (2002) 907–915.
[27] S.W. Chen, S.H. Wu, S.W. Lee, Interfacial reactions in the Sn-(Cu)/Ni, Sn(Ni)/Cu and Sn/(Cu,Ni) systems, J. Electron. Mater. 32 (2003) 1188–1194.
[28] C. Schmetterer, M. Rodriguez-Hortala, H. Flandorfer, Enthalpies of formation of $(Cu,Ni)_3Sn$, $(Cu,Ni)_6Sn_5$-HT and $(NiCu)_3Sn_2$-HT, JPEDAV 35 (2014) 429–433.
[29] P. Hermann, C. Biselli, D.G. Morris, Influence of heat treatments on microstructure and mechanical properties of Cu-15Ni-8Sn, Mater. Sci. Technol. 13 (1997) 489–496.
[30] P. Hermann, D.G. Morris, Relationship between microstructure and mechanical properties if a spinodally decomposing Cu-15Ni-8Sn alloy prepared by sparay deposition, Metall. Mater. Trans. A 25 (1994) 1403–1412.
[31] F. Sadi, C. Servant, Phase transformations and phase diagram at equilibrium in the Cu-Ni-Sn system, J. Therm. Anal. Calorim. 90 (2007) 319–323.
[32] V.M. López-Hirata, A.J. Arias-Pérez, M.L. Saucedo-Muñoz, A study of precipitation in Cu-15wt%Ni-8wt%Sn alloy, J. Mater. Sci. Lett. 18 (1999) 1697–1699.
[33] M.J. Diánez, E. Donoso, J.M. Criado, M.J. Sayagués, G. Diaz, L. Olivares, Study by DSC and HRTEM of the aging strengthening of Cu-Ni-Zn-Al alloys, Mater. Des. 92 (2016) 184–188.
[34] E. Donoso, R. Espinoza, M.J. Diánez, J.M. Criado, Microcalorimetric study of the annealing hardening mechanism of a Cu-2.8Ni-1.4Si (at%) alloy, Mater. Sci. Eng. A 556 (2012) 612–616.
[35] S. Sheibani, S. Heshmati-Manesh, A. Ataie, A. Caballero, J.M. Criado, Spinodal decomposition and precipitation in Cu-Cr nanocomposite, J. Alloys Compd. 587 (2014) 670–676.
[36] S. Sheibani, A. Ataie, S. Heshmati-Manesh, A. Caballero, J.M. Criado, Influence of Al_2O_3 reinforcement on precipitation kinetic of Cu-Cr nanocomposite, Thermochim. Acta 526 (2011) 222–228.
[37] T.D. Shen, C.C. Koch, Formation, solid solution hardening and softening of nanocrystalline solid solution prepared by mechanical attrition, Acta Mater. 44 (1996) 753–761.
[38] T. Klassen, U. Herr, R.S. Averback, Ball milling of systems with positive heat of mixing: effect of temperature in Ag-Cu, Acta Mater. 45 (1997) 2921–2930.
[39] N. Lourenço, H. Santos, Using differential scanning calorimetry to characterize the precipitation hardening phenomena in a Cu-9Ni-6Sn, J. Mater. Eng. Perform. 14 (2005) 480–486.
[40] L.H. Schwartz, S. Mahajan, J.T. Plewes, Spinodal decomposition in a Cu-9 wt% Ni-6 wt% Sn alloy, Acta Metall. 22 (1974) 601–609.